Supplemental Information

Subproject 1: Mechanism of NLRP1/CARD8 interaction with novel peptidases

We have recently completed structural studies on the DPP9-NLRP1 interaction (**Fig. 1A**) and the DPP9-CARD8 interaction. In collaboration with the Bachovchin Group at MSK, we found that PREP-L, another protein in the DPP/DASH family of peptidases, binds NLRP1 and CARD8 (**Fig. 1B**). Given that DPP9, PREP, and PREPL are all exhibit post-proline peptidase activity, we set out to purify these constructs using similar protocols (Ross et al. 2018). We were able to obtain homogeneous, monodisperse PREP-L and PREP (a homolog) from Sf9 insect cells. Since we noted a considerable difference in their elution volumes from a size exclusion column, we also performed SEC-MALS on PREP and PREPL, using DPP9 as a control. We determined that while PREP is a monomer, PREPL is a dimer (**Fig. 1C**). Because of its unknown function, size (~160 kDa), and predicted structural similarity to peptidases with globular folds, we proceeded with negative stain and then cryo-EM of the PREP-L dimer. Collection of a small 700-movie dataset yielded very well defined 2D classes (**Fig. 1D**), and we are still processing this dataset. However, we will likely need 1 full day of K3 collection (~4000 movies) in order to resolve sufficient detail for meaningful biological conclusions.

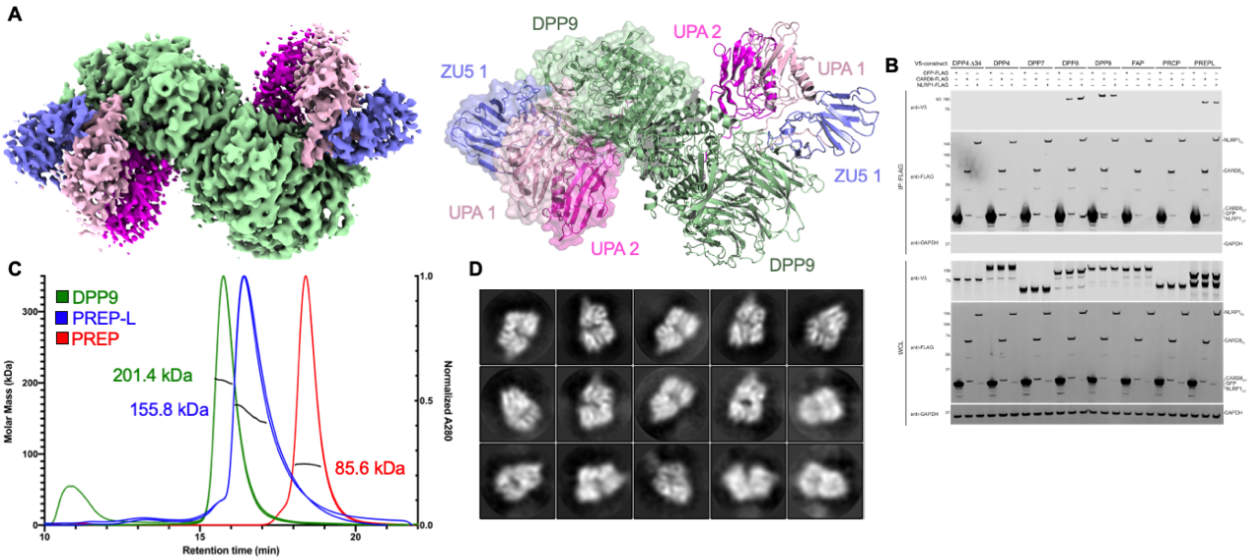

Figure 1. Preliminary data for PREP, PREP-L, and NLRP1. A) The NLRP1-DPP9 structure resolved at 3.5 Å resolution, indicating that NLRP1 can be purified and is well-behaved under cryo-EM. B) Co-immunoprecipitation indicating that PREP-L binds NLRP1 and CARD8. C) SEC-MALS of PREP (monomer), PREP-L (dimer), and DPP9 (dimer) indicating very well-behaved protein. D) PREP-L 2D classes from a small initial dataset (~700 micrographs) showing well-resolved features.

Subproject 2: Structural basis for NLRP3 inflammasome regulation

The first structure of monomeric NLRP3 in complex with NEK7 at 3.8 Å resolution (Sharif*, Wang*, Wang*, *et al*., *Nature*, 2019) provided the first glance of NLRP3 in an inactive form (**Fig. 2A**). Inspired by this progress, we proceeded to work on other conformations of NLRP3 and discovered its ability to form large oligomers, clearly visible on negative stain grids (**Fig. 2B**). The first cryo-EM dataset of 6000 micrographs resulted in a decent 3D reconstruction of an auto-inhibited, NLRP3 in the absence of NEK7 at 4.2 Å resolution (**Fig. 2C**). 2D classification, however, indicated complex heterogeneity, suggesting room for further sample improvement (**Fig. 2D**).

Furthermore, as a second part of this project, we were able to reconstitute NLRP3:BTK complex, which forms a distinct peak in SEC (**Fig. 2E**). The first cryo-EM grids, screened on the HMS Talos, looked promising and we are awaiting collection of a small initial dataset to estimate sample quality and to evaluate orientation coverage on the cryo-EM grids (**Fig. 2F**).

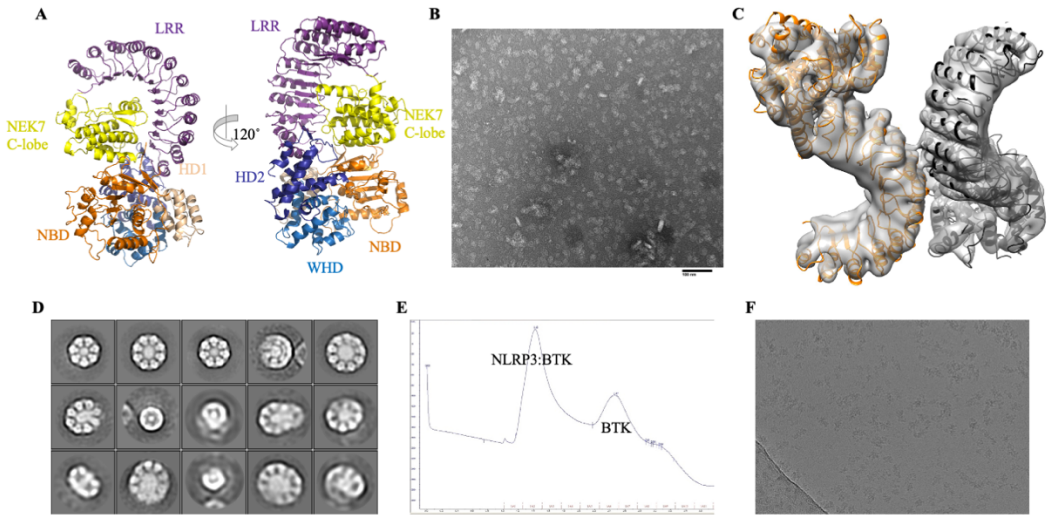

Figure 2. Figure 2. Preliminary data for NLRP3 subproject. (A) A structure of NLRP3:NEK7 complex (PDB 6NPY) (Sharif*, Wang*, Wang*, *et al.*, Nature, 2019). NEK7 (yellow) interacts with LRR (purple), NBD (orange) and HD2 (dark blue) domains of NLRP3. (B) Negative stain image (magnification 50K) of NLRP3 complex in oligomeric state. (C) A segment of NLRP3 oligomer resolved at 4.2 Å with fitted 6NPY NLRP3 model. (D) 2D classes of NLRP3 oligomer from Krios collection (~6000 micrograph dataset). (E) SEC of the NLRP3:BTK complex. (F) A representative micrograph of NLRP3:BTK complex (36K).

Subproject 3: Structural basis for NLRP6 inflammasome signaling

We have successfully expressed NLRP6 full-length or individual domains and determined the cryo-EM filament structure of the NLRP6 PYD (Shen *et.* al, *PNAS*, 2019). Through optimization of NLRP6 in complex with a binding partner, we have obtained particles that look homogeneous under negative stain EM (**Fig. 3D**). Initially we had difficulty in cryo-grid preparation in that the holes contained a very low particle density. After a series of optimization experiments, we now show that we can freeze grids with high monodisperse particle distribution (**Fig. 3A**). The initial data collection resulted in a moderate-resolution 3D reconstruction at 6.5 Å (**Fig. 3E**). However, we also experienced structure heterogeneity when we processed the initial dataset. For future optimization of the sample, we will consider a crosslinking strategy to stabilize the protein complex.

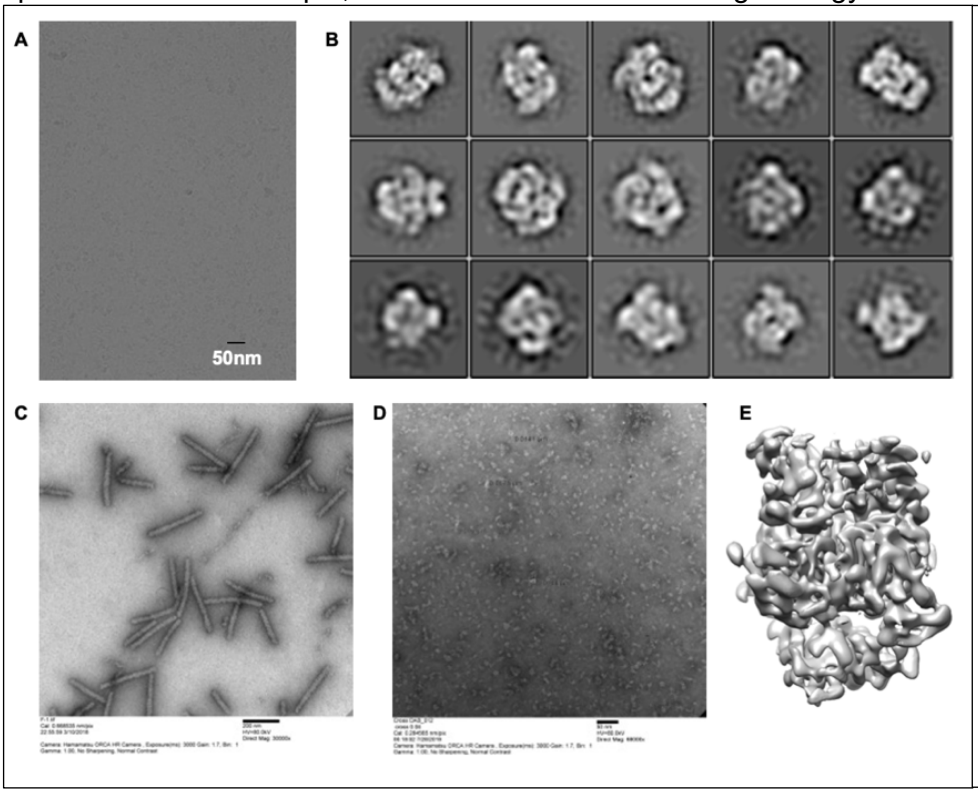

Figure 3. Preliminary data for the NLRP6 subproject. (A) Cryo-EM micrograph from Talos screening of the NLRP6-ligand complex. (B) 2D classes from initial data collection of the NLRP6/ligand complex, showing decent features of complex assembly. (C) Negative stain image of NLRP6-FL filament sample. (D) Negative stain image of NLRP6/ligand complex. (E) Initial 3D reconstruction of the N6/ligand complex, resulting in a moderate-resolution structure.

For the NLRP6-FL filament sample, we obtained promising negative stain EM results (**Fig. 3C**) and will therefore move on to sample assessment under cryo-EM prior to data collection.